Journal of Hazardous Materials 385 (2020) 121576

Contents lists available at ScienceDirect

Journal of Hazardous Materials

journal homepage: www.elsevier.com/locate/jhazmat

Nicosulfuron sorption kinetics and sorption/desorption on volcanic ash-derived soils: Proposal of sorption and transport mechanisms

Lizethly Caceres-Jensen[a,*,1], Jorge Rodriguez-Becerra[a], Mauricio Escudey[b,c], Jorge Joo-Nagata[d], Cristian A. Villagra[e], Valentina Dominguez-Vera[a], Angelo Neira-Albornoz[a,f], Maribel Cornejo-Huentemilla[a]

[a] Laboratorio de Físicoquímica&Analítica, Departamento de Química, Facultad de Ciencias Básicas, Universidad Metropolitana de Ciencias de la Educación, Avenida José Pedro Alessandri 774, Santiago, Chile
[b] Facultad de Química y Biología, Universidad de Santiago de Chile, Avenida Alameda Libertador Bernardo O'Higgins 3363, Santiago, Chile
[c] Center for the Development of Nanoscience and Nanotechnology, CEDENNA, 9170124, Santiago, Chile
[d] Departamento de Historia y Geografía, Facultad de Historia, Geografía y Letras, Universidad Metropolitana de Ciencias de la Educación, Avenida José Pedro Alessandri 774, Santiago, Chile
[e] Instituto de Entomología, Facultad de Ciencias Básicas, Universidad Metropolitana de Ciencias de la Educación, Avenida José Pedro Alessandri 774, Santiago, Chile
[f] Facultad de Ciencias Químicas y Farmacéuticas, Universidad de Chile, Santos Dumont 964, Independencia, Chile

GRAPHICAL ABSTRACT

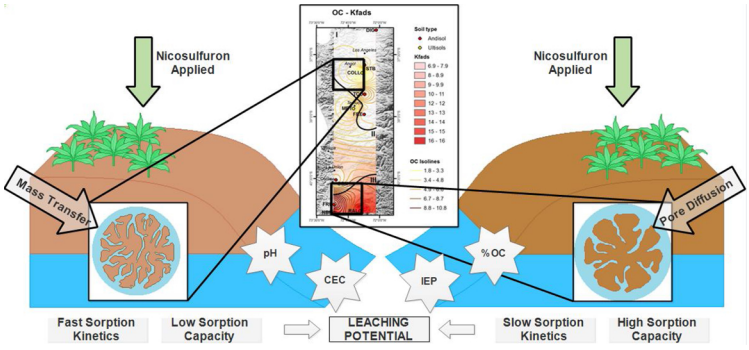

ARTICLE INFO

Editor: Deyi Hou

Keywords:
Herbicides
Sorption kinetics
Variable ash-derived soils
Principal component analysis

ABSTRACT

Nicosulfuron sorption/desorption kinetics were studied through batch sorption studies in ten volcanic ash-derived Andisol and Ultisol soils with acidic pH and variable surface charge. Two different kinetic models were used to fit the experimental data: i) Models to establish kinetic parameters (Pseudo-First and Pseudo-Second-Order), and ii) Models to describe solute transport mechanisms of organic compounds on sorbents (Intraparticle Diffusion, Dimensionless Intraparticle, Boyd, and Two-Site Nonequilibrium). Sorption kinetic data best fit the pseudo-second-order model. Application of these models to describe solute transport suggests that underlying mechanisms are complex in all soils due to: i) surface sorption, with mass transfers controlling sorption kinetics across the boundary layer; and ii) pore diffusion (i.e. intraparticle diffusion into macropores and micropores). The Freundlich model explained equilibrium sorption data in all cases ($R^2 > 0.9979$) with K_f values higher than those reported for different class of soils (6.85–16.08 $\mu g^{1-1/n}\, mL^{1/n}\ g^{-1}$). The hysteresis was significant in all

* Corresponding author.
E-mail address: lyzethly.caceres@umce.cl (L. Caceres-Jensen).
[1] www.pachem.cl.

https://doi.org/10.1016/j.jhazmat.2019.121576
Received 27 June 2019; Received in revised form 8 October 2019; Accepted 30 October 2019
Available online 06 November 2019
0304-3894/

studied soils. The lower sorption rate on Ultisols must be considered in regards to Nicosulfuron leaching potential.

1. Introduction

The principal process that affects the fate and transport of pesticides in soil and water is sorption from soil solution to soil particle active sites (Caceres-Jensen et al., 2018, 2019b). Sorption processes have considerable ecosystem impacts, influencing the availability of organic pollutants for plant uptake and microbial degradation and limiting pesticide transport in soils by reducing their concentration in the soil solution (Site, 2001). Sorption processes are described as complex processes involving a number of sequential mechanisms which determine, in a time-dependent fashion, the rate of sorption of organic pollutants (Caceres-Jensen et al., 2019a,b; Valderrama et al., 2008; Ayranci and Hoda, 2005; Tan and Hameed, 2017; Fernández-Bayo et al., 2008; Pojananukij et al., 2017). For instance: i) Liquid Film Diffusion (first stage) occurs within the boundary layer around the sorbent as readily available sorption sites rapidly uptake sorbates and continues in the liquid-filled pores (External Mass Transfer (EMT) steps) or along the walls of the pores of the sorbent (Internal MT (IMT) step s). These processes correspond to the transport of sorbates from the bulk phase to the external surface of adsorbent. ii) The first stage is followed by slow diffusion-immobilization in mesopores, micropores, or capillaries of the sorbent's internal structure (Inoue et al., 2004). This stage (Pore Diffusion or Intraparticle Diffusion (*IPD*)) involves the transport of sorbate from the external surface into the pores. iii) The third stage is the sorption-desorption reaction of solute in the inner surface of the sorbent through mass-action-controlled mechanisms, involving rapid uptake or surface reactions through interactions between solute and surface functional groups (chemisorption). In the agrochemical context, understanding sorption kinetics may provide important information related to weed control, crop toxicity, runoff, and carryover events and inform accurate estimations of biotic/abiotic environmental effects as well as decontamination efforts (Tan and Hameed, 2017; Inoue et al., 2004; Tournebize et al., 2013; Yu et al., 2010; Brown, 1990).

Sorption kinetics and sorption-desorption studies have rarely included volcanic ash-derived soils (VADS) (Tan and Hameed, 2017; Takahashi and Shoji, 2002; Caceres-Jensen et al., 2013). VADS are essential to the agricultural economies of several developing countries in Asia, Africa, Oceania and America (Shoji and Takahashi, 2002),

Table 1
Main physical and chemical properties and mineral composition of the ten Volcanic Ash-Derived soils (VADS) used in this study (Escudey et al., 2001).

Ultisols			Andisols							
	COLL*	MET	FRE	STB	OSN	DIG	TCO	RAL	NBR	FRU
Classification	Fine, Mesic, Xeric, Paleumult	Fine, Mesic, Paleumult	Medial, Mesic, Xeric, Placandept	Ashy, Medial, Mesic, Typic, Dystrandept	Medial, Mesic, Typic, Dystrandept	Medial, Thermic, Typic, Dytrandept	Medial, Mesic, Entic Dystrandep	Mesic, Umbric, Vitrandept	Ashy, Mesic, Hydric, Dystrandept	Medial, Isomesic, Typic, Placandept
Location	36°58'S; 72°09'W	38°34'S; 72°22'W	38°57'S; 72°36'W	36°50'S; 71°55'W	40°32'S; 73°05'W	36°53'S; 72°10'W	38º56'S; 72º36'W	41°32'S; 73°05'W	41°19'S; 73°06'W	41°06'S; 73°07'W
OC (%)	1.5	2.3	4.5	5.1	5.1	5.8	6.4	6.9	9.5	11.0
pH_{H2O} (1:2.5)	5.2	4.7	4.4	5.7	4.6	6.2	5.4	4.4	4.1	4.1
pH_{CaCl_2} (1:2.5)	4.7	4.8	5.0	5.3	4.6	5.5	5.2	4.6	4.3	4.9
****ΔpH**	−0.5	0.1	0.6	−0.4	0.0	−0.7	−0.2	0.2	0.2	0.8
CEC	8.7	9.3	7.1	10.3	9.8	11.8	12.1	7.1	10.3	9.5
Sand (%)	13.7	8.0	21.3	7.2	10.1	35.5	16.1	47.3	6.2	16.3
Silt (%)	40.7	56.7	54.2	66.5	50.9	45.1	58.2	38.5	66.2	63.9
Clay (%)	45.7	35.3	24.5	26.3	39.1	19.4	25.7	12.9	27.6	19.7
Fe_{PYRO} (%)	0.7	0.8	2.2	0.3	1.4	0.4	0.7	1.8	1.8	1.0
Fe_{OX} (%)	0.9	1.8	2.5	1.9	2.0	1.9	2.2	1.4	3.3	0.6
Fe_{DCB} (%)	6.2	7.1	4.3	5.3	3.0	3.5	3.9	1.4	5.1	0.6
IEP	2.0	2.5	3.1	3.8	2.1	2.6	2.9	3.3	3.3	2.9
Mineral										
Allophane			+ + + + +	+ + + + +	+ + + + +	+ + + + +	+ + + + +	+ + + + +	+ + + + +	+ + + + +
α-Cristobalite	+		+		+		+ +	+	+	+
Chlorite–AL				+				+ +		
Feldespars					+		+		+	
Ferrihydrite			+			+	+		+	
Gibbsite			+ +	+			+ +		+ +	
Goethite		+								
Halloysite	+	+ + + + +		+ +	+ + +	+ +				+
Kaolinite	+ + + + +									
Montmorillonite								+		
Organo-allophanic			+ +	+	+ +	+	+ +		+ +	+
Plagioclase					+	+ +		+ +		+
Quartz		+	+							
Vermiculite	+			+ +	+	+				+ +

* COLL (Collipulli), MET (Metrenco), FRE (Freire), STB (Santa Barbara), OSN (Osorno), DIG (Diguillin), TCO (Temuco), RAL (Ralun), NBR (Nueva Braunau) and FRU (Frutillar).

Fe_{PYRO}, Fe_{OX} and Fe_{DCB} represents Fe oxides extracted by pyrophosphate, acid ammonium oxalate and dithionite citrate bicarbonate solutions, respectively. + + + + + Represents dominant (> 50 %), + + + + represents abundant (20–50 %), + + + represents common (5–20 %), + + represents present (1–5 %) and + represents trace fraction (< 1 %).

**Δ pH= $pH_{CaCl_2\,(1:2.5)}$ − $pH_{H_2O\,(1:2.5)}$, where the soil surface net charge is negative for ΔpH<0 and positive when ΔpH>0.

Table 2
Uses (Caceres-Jensen et. al, 2019), properties, analytical detail and experimental procedures for Nicosulfuron (NS).

Pesticide name [CAS RN]	Formula	Molar Mass (g mol^{-1})	Use and APPR[a] (g ha^{-1})	pK_a[b]	K_{ow}[c]	S_w[d] (g L^{-1})	DT_{50}[e] (days)
1-(4,6-Dimethoxy-2-pyrimidinyl)-3-[3-(dimethylcarbamoyl)-2-pyridylsulfonyl] urea, 2-[(4,6-Dimethoxypyrimidin-2-ylcarbamoyl)sulfamoyl]-N,N-dimethylnicotinamide [111991-09-4]	$C_{15}H_{18}N_6O_6S$	410.41	Post-emergence herbicide and selective mode of action. The APPR of NS is very low (2-75) for weed control in corn.	2.0, 4.3 and 9.6	0.44 at *pH* 5.0; 0.0068 at *pH* 9.0.	(0.36 g L^{-1} at 25 °C *pH* 5.0; 12 g L^{-1} at 25 °C *pH* 7.0; 39 g L^{-1} at 25 °C *pH* 9.0)	26 (under aerobic conditions)

HPLC Analysis

HPLC mobile phase	Flow rate (mL min^{-1})	Injection volume (μL)	Wavelength (nm)	Temperature (°C)	Column	Detection limit (mg L^{-1})
70:30 (V/V) = AcN: water at *pH* 2.8	1	25	240	35°C	MultoHigh 100 RP C18 (150 mm × 4.6 mm ID, 5 μm).	0.009

Kinetics sorption studies				Sorption-desorption studies			
Soil/solution ratio	NS (mg L^{-1})	Contact time (min)	Temperature (°C)	Soil/solution ratio	NS (mg L^{-1})	Contact time (h)	Temperature (°C)
1:5 (2 g air dried soil, 10 ml solution)	5 (in 0.01 M $CaCl_2$)	5, 15, 30, 45, 60, 90, 120 and 180.	25±1	1:5 (2 g air dried soil, 10 ml solution)	**Sorption studies:** 5, 10, 15, 20 and 25 (in 0.01 M $CaCl_2$). **Desorption studies:** After the sorption equilibrium was reached of samples treated at 25 mg L^{-1}, 5 mL of supernatant solution was replaced with 5 mL of herbicide-free 0.01 M $CaCl_2$ solution, and then samples were shaken. The same step was repeated for four consecutive times.	24 2	25±1

[a] APPR = Application rate (Ukrainczyk and Rashid, 1995).
[b] *pKa* = dissociation constant (Ukrainczyk and Rashid, 1995).
[c] K_{ow} = Octanol/water partition coefficient (Maqueda et al., 2017).
[d] S_w = Solubility in water (Gonzalez and Ukrainczyk, 1996).
[e] DT_{50} = Half-life time in soil (Maqueda et al., 2017).

particularly in regions with geochemical characteristics dominated by active and/or recently extinct volcanic activity. Such is the case for the geomorphology of the Andean Plate, where most of Chilean territory lies (Shinohara and Witter, 2005; Rivera et al., 2012; Vergara et al., 2004; Stern, 2004). Among VADS, Andisols and Ultisols are the most abundant (Caceres-Jensen et al., 2018) and widespread in Central-Southern Chile (from 19° to 56 °S latitude), accounting for approximately 69 % of the country's arable land.

Previous studies of sorption kinetic of herbicides on VADS indicate that sorption is a non-equilibrium sorption process (time-dependent sorption or non-ideal sorption) (Caceres-Jensen et al., 2013, 2018, 2019b; Caceres et al., 2010). Physical and chemical non-equilibrium sorption can result from factors such as diffusive mass transport resistances, non-linearity in sorption isotherms, sorption-desorption non-singularity and rate-limited sorption reactions (Caceres-Jensen et al., 2019b; Villaverde et al., 2009). Both the rate-limited diffusion of the sorbate from bulk solution to the external surface of the sorbent and the rate-limited diffusion within mesopores/micropores of the soil constituents matrix occur before the equilibrium is reached. Differences observed in the sorption kinetics of ionizable herbicides on VADS have been attributed to differences in soils constituents, such as *OC* and mineral composition. Ionizable herbicides (e.g., phenoxy acids, triazines, sulfonylureas, imidazolinones) are particularly common and represent the largest major group of soil-applied herbicides (Kah and Brown, 2006). Nicosulfuron (NS) is an active ingredient of Accent (DuPont®) and classified as a member of the sulfonylureas (SUs) herbicides. This herbicide differs from most other SUs by the presence of the pyridine ring in place of the benzene on the left side of the sulfonylurea bridge as well as by the presence of a carboxamide group on the pyridine ring (Ukrainczyk and Rashid, 1995). Contamination of surface and groundwater with SUs is a major concern due to the intensive and widespread use of these chemicals in agricultural and urban areas (Caceres et al., 2010; Azcarate et al., 2015; Cáceres-Jensen et al., 2010). Establishing sorption kinetic parameters using kinetic models, as well as elucidating sorption mechanisms of solute transport in soil, are two aims fundamental to understanding and mitigating groundwater contamination with SUs. While the potential for NS groundwater contamination is expected to be lower than other corn herbicides with higher application rates, SUs are weakly adsorbed to soil, with sorption thought to decrease with elevated pH and increasing anionic species in solution. Consequently, SUs mobility in soil usually increases when *pH* increases and soil *OC* decreases. Taken together, these observations suggest that if SUs sorption increases with time, their availability and transport to groundwater will decrease.

Considering the limited literature on the behavior of NS in VADS and the widespread, increasing use of SUs in world's agriculture, this work aimed to establish the sorption kinetics of NS in ten different agricultural VADS from Chile, including time required to reach equilibrium, matrix sorption capacity, and the order and rate of the sorption. Seven different solute sorption mechanism models were evaluated considering model restrictions, soil descriptor by mean Principal Component Analysis (PCA) to investigate the mechanisms involved in NS sorption on VADS and spatial models to investigate the soils properties variability at regional scale. These kinetics studies were complemented with batch sorption-desorption studies of NS on VADS. Together, the sorption-desorption type and kinetics sorption models described herein may be used to support development and validation of computer simulation transport models on VADS or serve to increase quality sorption data for developing reliable models to predict pesticide sorption on VADS to prevent potential contamination of water resources (Valenzuela Riquelme et al., 2010; Cáceres-Jensen, 2010).

2. Materials and methods

2.1. Soil samples

The VADS were collected from the 0 to 15-cm layer in agricultural regions of southern-central Chile (Table 1). The soil OC content was determined by the Walkley-Black method (Allison, 1965). pH was measured in soil suspensions with a soil to water ratio of 1:2.5 (w/v). Cation Exchange Capacity (CEC) was determined by the method outlined by (Blake (1965), corresponding to the sum of Na, K, Mg, and Ca concentrations in the ammonium acetate extracts. The isoelectric point was determined through electrophoretic measurements. The mineralogy and chemical composition of these soils have been previously described (Pizarro et al., 2003).

2.2. Chemicals

Analytical reference standard NS (99.7 %, purity) was obtained from Sigma-Aldrich (Table 2). All reagents used were analytical or HPLC grade.

2.3. Kinetic sorption experiments, sorption-desorption experiments and models

Analytical procedures and experiments description are showed in Table 2. Detailed analytical procedures and experiments descriptions are given in SI section. The Table 3 shows the theoretical and empirical description for each model.

2.4. Spatial models

For the spatial interpolation of soil values, ArcGIS 10.4.1 software with Inverse Distance Weighting (IDW) method was used (Denton et al., 2017; Robinson and Metternicht, 2006). A Digital Elevation Model (DEM) was created to present K_f values.

3. Results and discussion

3.1. Characterization of soils

The Andisols used in this study presented high *OC* content with mineralogy dominated by allophane (Table 1). The Ultisols exhibited lower *OC* than Andisols, but higher total iron oxide content, presenting an acidic pH (Table 1). Andisols presented variable surface charge due to inorganic minerals (goethite, ferrihydrite, gibbsite and allophane; Table 1) and organic matter (*OM*) through the humus-Al/Fe complexes with amphoteric characteristics and the dissociation of its functional groups (mainly carboxylic and phenolic). Ultisols presented little or no variable surface charge due to the dominance of crystalline minerals (halloysite and kaolinite, Table 1). PCA was used to assess the degree of difference between VADS (Figs. 1 and SI 1). Figs. 1b and d indicate that chemical properties differentiated VADS grouped around PC1 (e.g. DIG, OSN and FRE; TCO, STB and RAL).

3.2. Sorption kinetics

3.2.1. Pseudo-first order (PFO) and pseudo-second order (PSO) models

The experimental q_{max} values were not in agreement with those calculated by the *PFO* model (Eq. 2, Table 3) despite the fairly high R^2 values (> 0.9243) (Fig. SI 3, Table 4). Instead, higher R^2 values were obtained with the *PSO* model (> 0.9995), more accurately characterizing NS sorption experimental data across all time intervals (Fig. 2). A low C_0 of NS (5 μ g mL^{-1}) was chosen to increase the overall sorption rate, as the k_2 constant is a time scale factor that decreases when C_0 increases (Table 3) (Tan and Hameed, 2017). Accordingly, the kinetic experiments demonstrated that this system obeys the *PSO* model (Eq. 3,

Table 3
Models used to describe kinetic, sorption and desorption of Nicosulfuron (NS) on Volcanic Ash-Derived Soils (VADS)*.

Equation	Parameters	Theoretical and Empirical Description
Adsorbed quantity:	$q_t = C_s$: Adsorbed quantity (μg g^{-1}) at any soil-solution contact time t (min) for kinetic sorption experiments. C_0: Initial concentration of NS in solution. C_t: Concentration of NS in solution at any soil-solution contact time t (min) V/M: Solution/soil ratio.	The adsorbed quantity is obtained from a mass balance between initial and equilibrium concentration of NS in solution. This equation is valid when degradation and precipitation are negligible during the sorption process.
Sorption kinetic		
Pseudo-first-order (*PFO*) model (Caceres-Jensen et al., 2013):	q_{max}: is the maximum sorbed amount (μg g^{-1}). k_1: Rate constant (min^{-1}).	This equation fits better at high C_0 values. The k_1 is a combination of sorption (k_a) and desorption (k_b) rate constants (Azizian, 2004). Its magnitude is influenced by experimental conditions (pH and temperature) and particle size (small particle size imply large values of k_1).
Pseudo-second-order (*PSO*) model (Azizian, 2004; Ruiz et al., 2010; Önal, 2006; Wankasi et al., 2006; Kumar et al., 2005; Hameed and El-Khaiary, 2008; Ho, 2006):	k_2: Rate constant (g μg $^{-1}$ min^{-1}). **Derived parameters from Eq. 3:** h: Initial sorption rate (g μg^{-1} min^{-1}), $h = k_2 q_{max}^2$. $t_{1/2}$: Half-life time (min), $t_{1/2} = 1/(k_2 q_{max})$.	Frequently used to establish kinetic parameters of chemisorption process for different solutes on different sorbents from liquid solutions (Caceres-Jensen et al., 2013). This equation fits better at low C_0 values (Azizian, 2004). The k_2 is a complex function of C_0, because is a time scale factor that decreases when C_0 increases. This model assume that sorption capacity could be proportional to the number of active sites occupied on the soil (Fernández-Bayo et al., 2008).
Solute sorption mechanism		
Elovich model (Önal, 2006; Rudzinski and Panczyk, 2000): *Dimensionless Elovich* model (Wu et al., 2009a):	α: Initial sorption rate (μg g^{-1} min^{-1}). β: Number of sites available for the sorption (g μg $^{-1}$), related to the extent of surface coverage and activation energy for chemisorptions. $(1/\beta)$: sortion rate constant during the slow phase of the reaction. $(1/\beta)ln(\alpha\beta)$: Amount adsorbed during the initial fast phase reaction. $R_E = 1/(q_{ref}\,\beta)$: Approaching equilibrium factor. t_{ref}: Longest time in the sorption process (so, $t_{ref} = t$ at equilibrium). q_{ref}: Solid phase concentration at $t = t_{ref}$ (so, $q_{ref} = q_{max}$).	This equation has been proposed to describe *second order* kinetics only for systems with a heterogeneous adsorbing surface and also it shows that along with surface adsorption chemisorption is also a dominant phenomenon taking place. The deviations of *Elovich* model at high surface coverage could be a consequence that this model neglects the effects of the simultaneously occurring desorption. At low surface coverage, this equation might be applied only in cases of strongly heterogeneous surfaces. When $R_E > 0.3$, the curve rises slowly (Zone I), in the range $0.3 > R_E > 0.1$, the curve rises moderately (Zone II); in the range $0.1 > R_E > 0.02$, the curve rises rapidly (Zone III); and when $R_E < 0.02$, the curve reaches equilibrium instantly (Zone IV).
Intraparticle Diffusion (*IPD*) model (Önal, 2006; Kumar et al., 2005): *Dimensionless Intraparticle Diffusion* (*DIPD*) model (Wu et al., 2009b):	$k_{int\,i}$: Rate constant of the step i (μg g^{-1} $min^{1/2}$). C_i: Thickness of the boundary layer in the step i (μg g^{-1}). R_i: Initial sorption factor in the step i (if $q_{ref} = q_e$, the applicability of dimensionless *IPD* model is limited to only one step).	The intercept *C* is related to the extent of the boundary layer effect, and is proportional to the boundary layer thickness. Such intercept has been taken as a component representing the initial sorption on external sites (Tan and Hameed, 2017; Inoue et al., 2004). When $C_1 = 0$, *IPD* is the most important rate process controlling sorption; $C_1 > 0$, *IPD* was not the only rate controlling step. Thus, the first step must be attributed to the EMT across the boundary layer controlled by Liquid Film Diffusion. The larger the intercept the greater boundary layer effect (Fernández-Bayo et al., 2008), positive intercepts indicating a rapid sorption on adsorbents with a wide distribution of pore sizes (Wu et al., 2009b). The initial sorption can be weak (zone I, $1 > R_i > 0.9$), medium (zone II, $0.9 > R_i > 0.5$), strong (zone III, $0.5 > R_i > 0.1$) or complete (zone IV, $R_i < 0.1$) regarding the equilibrium sorption.
Boyd model (Boyd et al., 1947):	$B = -D_2\pi^2/r^2$: Empirical constant related with the Effective Diffusion coefficient (D_2) and the Effective Particle Size (r^2) for the sorption process.	The calculated Bt values can be analyzed in a linear plot of *Bt* versus *t*. If the plot of *Bt* versus *t* (Bt= C+ k*t) is linear with C = 0, the rate of MT is controlled by *IPD*. If the plot is nonlinear or linear but C≠ 0, the film diffusion or chemisorption controls the sorption rate (Caceres-Jensen et al., 2013).
Two-Sites Nonequilibrium (*TSNE*) model (Villaverde et al., 2009; Cáceres-Jensen et al., 2010; Wu et al., 2009b; Nkedi-Kizza et al., 2006):	C_t: Solute concentration at any time (μg mL^{-1}). C_{in}: Initial added solute concentration (μg mL^{-1}). R: Retardation factor, proportional to the sorption strength. β: Fraction of retardation for Type 1 sites (where sorption is assumed to be instantaneous). k_{des}: First-order desorption rate constant for desorption from the Type 2 sites (where sorption is considered time-dependent) (h^{-1}). **Derived parameters from Eq. 9:** K: Linear sorption partition coefficient at equilibrium (mL μg^{-1}); K= (R−1)*V/M.	The sorption parameters, k_{des} and K has been inversely related for neutral organic chemicals in soils and sediments (Nkedi-Kizza et al., 2006). The k_{des} is considered as a parameter which combines indiscriminately several processes, such as intra-OM diffusion and delayed *IPD* that control MT of sorbate into the OM complex.

(*continued on next page*)

Table 3 (*continued*)

Equation	Parameters	Theoretical and Empirical Description
	F: Fraction of the total sorption in the Type 1 sites when the system is in equilibrium, F= (βR− 1)/(R− 1). k_s: Rate constant for EMT, calculated from the slope of linearization in the plot of C/C_{in} vs time t at initial time intervals.	
Sorption-desorption process		
Sorbed and desorbed fraction:	%ads: Sorbed fraction (%) at equilibrium. %fast ads: Sorbed fraction (%) during the EMT. %slow ads: Sorbed fraction (%) during the *IPD*. C_e: Equilibrium concentration of NS in solution.	The sorbed fraction can be calculated by mean of *IPD* model, if different steps are present during the sorption process.
Linear model:	K_d: Linear soil-solution distribution coefficient. **Derived parameters from Eq. 12:** K_{oc} (from K_d) = 100*K_d/%OC: The *OC* distribution coefficient from K_d.	The *Linear* model is useful to describe sorption when the process is independent of the solute concentration.
Freundlich model:	K_f: *Freundlich* constant. 1/n: *Freundlich* sorption coefficient. **Derived parameters from Eq. 13:** K_{foc}: The *OC* distribution coefficient from K_f. K_{foc} = 100*K_f/%OC. *H*: Hysteresis coefficient for the sorption loop (des: desorption, ads: sorption). $H = (1/n_{des})/(1/n_{ads})$.	The *Freundlich* model presumes a heterogeneous surface (Appel, 1973). The single K_f term implies that the energy of sorption on a homogeneous surface is independent of surface coverage (Sparks, 2003). In this sense, the energy of binding is the same for the adsorptive sites, and interactions between adsorbed atoms do not exist (Appel, 1973). The *n* coefficient is related to the surface heterogeneity, magnitude and diversity of energies associates with the sorption process (Site, 2001; Maqueda et al., 2017). If 1/ n> 1, the sorption process shows a cooperative sorption, strong intermolecular attraction within the adsorbent layers, penetration of the solute in the adsorbent, and monofunctional nature of the adsorbate (Site, 2001). If 1/ n= 1, *Freundlich* model is equivalent to *Linear* model indicating low heterogeneity among the sites of the sorbent (Maqueda et al., 2017); If 1/ n< 1, the relative sorption decreases when the concentration increases indicating that the sorption firstly occurred on the higher energy sites of sorption, followed by the low energy sites (Okada et al., 2016). In this regards, the marginal sorption energy decreases with increasing surface concentration (Site, 2001).

* Goodness-of-fit (higher values of determination coefficients (R^2), lower standard error (SE) for each parameter), relationship between the theoretical basis for each sorption kinetic model were used as criteria to define the most suitable model to describe NS sorption kinetics and NS transport mechanisms on VADS. Complementary, the accuracy to predict q_{max} (from *pseudo-first* (*PFO*) and *pseudo-second* (*PSO*) order models) and K_d (from *Two Site Non-Equilibrium* (*TSNE*) model) were used.

Table 3) for the entire sorption period and thus supports the model's assumption that NS sorption is due to chemisorption on VADS (Table 3) (Riahi et al., 2017) with a rate constant that is function of C_0 of NS (Azizian, 2004).

The values of q_{max} estimated by the *PSO* model agree well with the experimental q_{max} values with low standard error (Table 4). NS presented the highest q_{max} in NBR (high *OC* and silt content, Fig. SI 2, Table 1) and lowest q_{max} in FRE (low *OC* and high silt content, Table 1). A positive correlation between *OC* content and q_{max} was observed for Andisols (Table SI 2). The fitting curve overestimated the q_{max} values calculated for FRE, STB, OSN, DIG, TCO and FRU and underestimated the q_{max} values calculated for COLL, MET, RAL and NBR. These results suggest that other soil properties such as silt and clay content, which are usually masked by the *OC*, play an important role in NS sorption on VADS.

Caceres-Jensen et al. (Cáceres-Jensen et al., 2010; Cáceres-Jensen, 2010) applied the *PSO* model to characterize the overall sorption rate of Metsulfuron-Methyl (MSM) on Andisols and Ultisols. The lowest q_{max} values were observed for Ultisols. Comparing the q_{max} obtained from MSM and NS on VADS, both herbicides presented the highest q_{max} on NBR due to its high content of *OC* (Table 1) (Escudey et al., 2001). This coincides with the notion that adsorbent properties including texture and surface chemistry influence the sorption process, while sorbate properties such as size and functional groups are also considered important (Tan and Hameed, 2017; Ioannou and Simitzis, 2009; Ruiz et al., 2010). Specifically, small adsorbate size reduces the MT effects, resulting in large k_2 values.

For Andisols, a negative correlation was observed between k_2 and q_{max} as well as *OC* content and k_2 (Table SI 2). Soils structured with high *OC* content have demonstrated slower sorption rates compared to dispersed soils with low *OC* content (Site, 2001). For all VADS except FRE, STB, OSN and DIG, a positive correlation was exhibited between clay/OC and k_2 (Table SI 2). The fitting curve overestimated the k_2 values calculated for FRE, STB, OSN and DIG. The FRE soil (Andisol with lowest *OC* content and high ratio of silt/ *OC* and clay/ *OC*) showed the highest k_2 value followed by COLL (lowest *OC* content and highest ratio of silt/ *OC* and clay/ *OC* ; Tables 1 and 4). The highest k_2 and *h* values observed in FRE and COLL soils suggest that NS moving rapidly down the soil profile should be easily and firmly retained on clay minerals surfaces. (Ukrainczyk and Rashid, 1995) In this context, the highest *h* and high q_{max} values for NS on COLL are interesting outcomes, given that this Ultisol presented negative net charge ($\Delta pH = pH_{CaCl_2} - pH_{H_2O} = -0.5$, Table 1). NS should be principally in the anionic form at the *pH* of COLL, according to its *pKa* values (Table 2).

The sorption of insecticides and herbicides on inorganic sorbents (kaolinite, sand) has generally been found to be very fast (minutes) (Site, 2001). Caceres-Jensen et al. (Cáceres-Jensen et al., 2010; Cáceres-Jensen, 2010) evaluated MSM (*pKa* = 3.3) sorption kinetics on COLL applying the *PSO* model. In contrast to NS, these SUs exhibit a benzene ring instead of pyridine on the left side of the sulfonylurea bridge and feature a methoxycarbonyl group at the ortho-position of the benzene

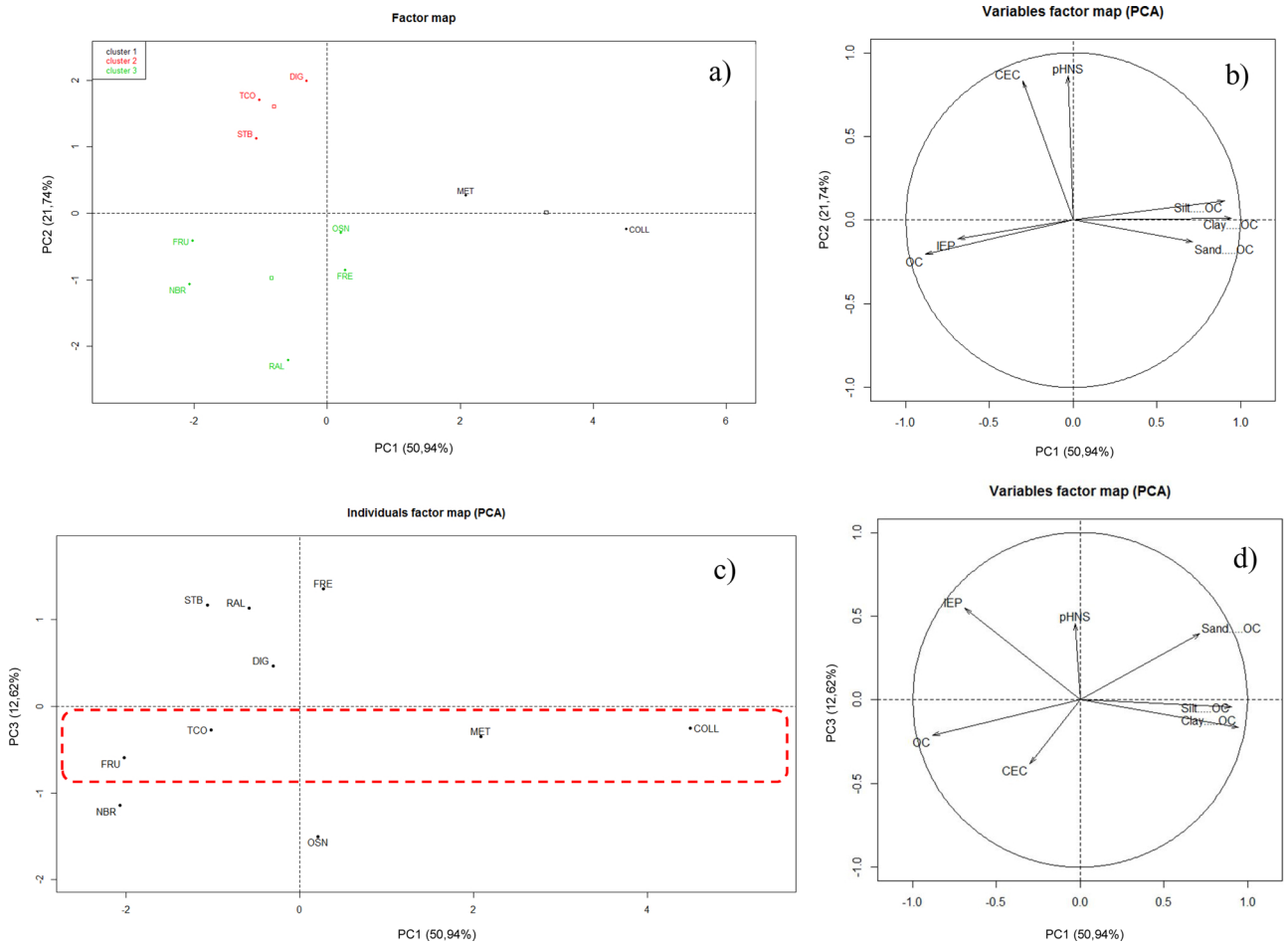

Fig. 1. Principal Component Analysis of NS on VADS. Scores (a) and loading (b) plots from Principal Component Analysis.

ring instead of a carboxamide group. MSM exhibits low values for q_{max} (6.95 μg g^{-1}), k_2 (8.7 ± 0.7 × 10^{-3} g μg^{-1} min^{-1}) and h (0.543 × 10^{-3} g μg^{-1} min^{-1}) on COLL. Comparing these results, NS sorption is two orders of magnitude faster than MSM, which is an unexpected behavior on negatively charged soils. Sorption kinetics of NS in VADS with a high clay/ OC ratio and negative net charge (COLL, $\Delta pH = -0.5$, % fast ads= 92.62; STB, $\Delta pH = -0.4$, % fast ads= 93.06 and DIG, $\Delta pH = -0.7$, % fast ads= 90.90; Tables 1, 4 and 5) are faster than in VADS with low ratio of clay/ OC and positive net charge (RAL, $\Delta pH = 0.2$, % fast ads= 87.96; NBR, $\Delta pH = 0.2$, % fast ads= 79.15 and FRU, $\Delta pH = 0.8$, % fast ads= 77.05; Tables 1, 4 and 5). Rapid NS sorption on negatively charged soils could be result from its interaction with clay minerals (Table 1).

Ukrainczyk et al. (Ukrainczyk and Rashid, 1995) suggested two hypothesis: i) NS can produce a zwitterion at the pH of soil solution, or ii) the minerals' surface acidity can catalyze rapid hydrolysis of NS. Notably, in our assays no degradation products were detected in soil solution extracts after 16 h of shaking. This result agrees with previous findings by Sabadie, J. (Sabadie, 2002), suggesting that the second hypothesis is unlikely given that only slow degradation of NS was observed on various oven-dried minerals.

Based on the textural characteristics of VADS, different values for k_2 and h would be expected. The differences were more remarkable in the early stages of NS sorption on VADS, as inferred from h and $t_{1/2}$. The soils COLL and FRE presented the highest h and lowest $t_{1/2}$ values (Table 4). The elapsed time for NS half uptake in COLL and FRE (0.7 min) increased by more than five times (3.2 min) in TCO and FRU. This result suggests that in COLL and FRE, film diffusion should initially contribute highly to EMT, resulting in an increased concentration gradient between NS in solution and NS on the soil surface through of the high number of active sites accessible. The NS fraction, with short $t_{1/2}$ and moderate adsorption on structured soils, could therefore percolate into ground water (Huentemilla, 2015) with rapid non uniform leaching (macropore or preferential flow) (Köhne et al., 2009).

3.3. Solute transport mechanism

3.3.1. Elovich model

The α values (Eq. 4, Table 3) are inconsistent with those calculated by the *PFO* model (h values, Table 4) despite the fairly high R^2 values (> 0.9658) (Fig. SI 3, Table SI 3). The SI includes a detailed analysis of the *Elovich* model.

3.3.2. Intraparticle diffusion (IPD) model

This model (Eq. 6, Table 3) was used as a first approach to discern between the limiting sorption step and *IPD* transport mechanism during NS sorption on VADS. Fig. 3 shows the *IPD* model plot for NS sorption on all soils. It is clear that q_t vs $t^{1/2}$ plots are multilinear in all VADS, where the NS sorption tends to be followed by three distinct steps. The first sharper step is attributed to boundary layer diffusion of NS molecules. The second stage describes the gradual sorption where IPD is rate limiting. The third step corresponds to the final equilibrium stage (Cáceres-Jensen et al., 2010, 2013). The presence of more than one sorption step has been related to the nature of sorption sites (i.e. OC, mineral) and/or pesticide accessibility (Caceres-Jensen et al., 2018, 2019; Inoue et al., 2004).

The first linear section passes far from the origin for all VADS ($C_1 > 0$; $R^2 > 0.8631$, Table 4). The largest C values were observed on

Table 4
Kinetic parameters predicted from Pseudo-First Order model, Pseudo-Second Order model, Intraparticle Diffusion, Dimensionless Intraparticle Diffusion, Boyd model and non-linear analysis for Two-site non-equilibrium (TSNE) model.

Parameters	COLL	MET	FRE	STB	OSN	DIG	TCO	RAL	NBR	FRU
q_{max} (exp.)	15.2	15.4	14.3	15.6	14.5	17.5	19.2	26.8	31.9	29.3
Pseudo-First Order										
q_{max} (μg g^{-1})	0.7±0.1*	1.2±0.1	0.6±0.1	0.9±0.1	0.8±0.1	1.6±0.1	4.9±0.3	2.5±0.2	5.4±0.5	5.3±0.5
k_1 (min^{-1})	0.04±0.07	0.05±0.06	0.04±0.11	0.03±0.07	0.04±0.09	0.07±0.07	0.05±0.06	0.04±0.06	0.05±0.06	0.04±0.05
R^2	0.9243	0.9817	0.9915	0.9698	0.9890	0.9918	0.9707	0.9435	0.9838	0.9556
Pseudo-Second Order										
q_{max} (μg g^{-1})	15.2±0.0	15.5±0.0	14.4±0.0	15.7±0.0	14.6±0.0	17.6±0.0	19.4±0.2	26.9±0.1	32.2±0.2	29.5±0.3
k_2 (g μg $^{-1}$ min^{-1})	0.10±0.02	0.06±0.01	0.11±0.03	0.06±0.02	0.07±0.02	0.06±0.01	0.02±0.00	0.02±0.01	0.01±0.00	0.01±0.00
R^2	1.0000	1.0000	1.0000	0.9999	1.0000	1.0000	0.9996	0.9999	0.9998	0.9995
h (g μg $^{-1}$ min^{-1})	22±5	15±3	22±6	16±5	15±4	17±4	6±1	18±5	12±2	9±2
$t_{1/2}$ (min)	0.7±0.2	1.1±0.2	0.7±0.2	1.0±0.3	1.0±0.2	1.0±0.2	3.2±0.7	1.5±0.4	2.6±0.5	3.2±0.9
K_d (exp.)	6.5	7.1	6.0	6.8	6.3	7.9	12.8	13.2	20.4	20.5
Intraparticle Diffusion										
$k_{int\,1}$ (μg g^{-1})	0.14±0.01*	0.15±0.01	0.06±0.00	0.11±0.01	0.10±0.00	0.16±0.01	0.43±0.04	0.31±0.04	0.67±0.06	0.63±0.10
C_1 (μg g^{-1})	14.0±0.0	14.0±0.1	13.7±0.0	14.5±0.1	13.5±0.0	15.9±0.1	14.7±0.3	23.5±0.2	25.2±0.4	22.0±0.6
R^2	0.9884	0.9111	0.9908	0.9583	0.9876	0.9700	0.9101	0.8631	0.9156	0.8696
$k_{int\,2}$ (μg g^{-1})	0.03±0.00	0.04±0.00	0.03±0.00	0.06±0.00	0.04±0.00	0.02±0.00	0.16±0.01	0.15±0.01	0.19±0.01	0.32±0.01
C_2 (μg g^{-1})	14.7±0.0	14.9±0.0	14.0±0.0	14.8±0.0	14.0±0.0	17.2±0.0	17.0±0.1	24.7±0.2	29.3±0.1	25.1±0.1
R^2	0.9835	0.9973	0.9951	0.9983	0.9912	0.9202	0.9796	0.9672	0.9842	0.9898
Dimensionless Intraparticle Diffusion										
R_i ($min^{0.5}$)	0.05	0.07	0.04	0.06	0.06	0.07	0.19	0.10	0.16	0.19
R^2	0.8066	0.8014	0.9489	0.9291	0.9268	0.8146	0.8532	0.8297	0.8213	0.8488
Boyd										
C	2.60±0.10	2.10±0.06	2.73±0.03	2.41±0.05	2.35±0.03	1.89±0.06	1.16±0.05	1.89±0.10	1.30±0.05	1.21±0.07
k (min^{-1})	0.02±0.00	0.02±0.00	0.02±0.00	0.01±0.00	0.02±0.00	0.03±0.00	0.02±0.00	0.02±0.00	0.02±0.00	0.02±0.00
R^2	0.9246	0.9811	0.9925	0.9703	0.9894	0.9907	0.9813	0.9436	0.9839	0.9555
Two Site Nonequilibrium										
K(mL g^{-1})	6.48±0.02	6.84±0.06	5.99±0.02	6.77±0.06	6.28±0.03	7.87±0.05	12.40±0.55	12.86±0.20	19.88±0.58	19.40±1.07
F	0.88±0.01	0.83±0.01	0.92±0.00	0.88±0.01	0.88±0.00	0.83±0.01	0.53±0.03	0.76±0.02	0.57±0.03	0.53±0.04
k_{des} (h^{-1})	1.99±0.24	1.50±0.36	0.95±0.07	1.21±0.27	1.14±0.12	1.50±0.20	1.12±0.28	1.81±0.45	1.36±0.27	1.18±0.37
R^2	0.9885	0.9872	0.9773	0.9686	0.9930	0.9872	0.9574	0.9509	0.9697	0.9317
k_s (h^{-1})	0.03±0.00	0.03±0.00	0.01±0.00	0.03±0.00	0.02±0.00	0.03±0.00	0.12±0.03	0.05±0.01	0.10±0.02	0.10±0.02
R^2	0.9512	0.8833	0.9954	0.8972	0.9489	0.9044	0.7943	0.8056	0.8237	0.7628

* Standard error.
*Standard error (duplicate).

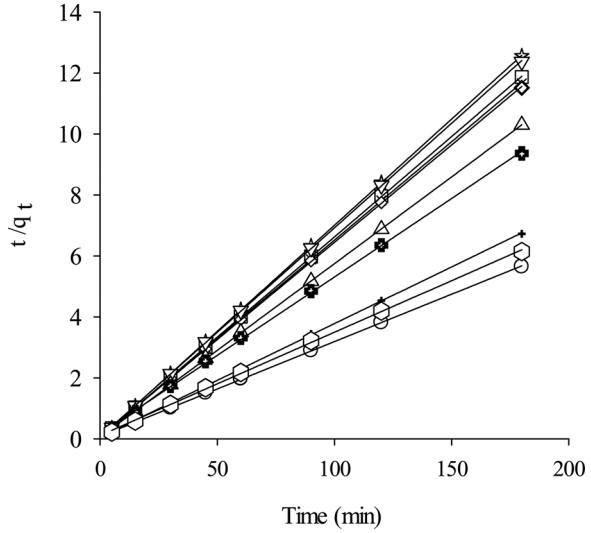

Fig. 2. Sorption kinetics of NS on VADS: COLL (□), MET (×), FRE (★), STB (◇), OSN (▽), DIG (△), TCO (✚), RAL (+), NBR (○) and FRU (+). Symbols represent the experimental data while lines represent the theoretical curves described by the *Pseudo-Second Order*.

TCO, RAL, NBR and FRU indicating high initial NS sorption (mg g^{-1}) with diffusion through the solution to the external surface on these soils through the thick boundary layer (first steps) (Caceres-Jensen et al., 2018; Tan and Hameed, 2017; Caceres-Jensen et al., 2019). The low h values exhibited in these soils were due to the high External Resistance MT (ERMT) surrounding NS onto sorbent during this early sorption stage (Table 4). ERMT surrounding the particles is presumed to be significant only in the early stages of sorption where the linear rate is initially steeper (Fig. 3) (Valderrama et al., 2008), and the initial time depends on variables including solute concentration, temperature, and sorbent particle size. C decreased with increasing soil surface heterogeneity indicating a small ERMT surrounding the adsorbent particle on COLL, MET, FRE, STB, OSN and DIG. A positive correlation was found between OC and C_1 and C_1 and $kint_1$ (Table SI 2). Previous work has related the degree of heterogeneity to textural properties (porosity) and chemical factors (composition) of adsorbents (Ruiz et al., 2010), observing that C values decreased when surface heterogeneity increased in chemically modified adsorbents.

The first linear section (k_{int1}, second step) accounted for the stage of gradual NS sorption, where EMT across the boundary layer and *IPD* through macropores were rate limiting factors. The second linear section (k_{int2}, third step) accounted for gradual NS sorption on micropores until the final equilibrium stage. In work by Caceres-Jensen et al. (Cáceres-Jensen et al., 2010; Cáceres-Jensen, 2010) regarding MSM sorption kinetics on VADS, the first linear plot passed near to the origin only for Ultisols ($R^2 > 0.97$). Similarly, *IPD* was the most important rate process controlling MSM sorption on Ultisols.

In the present work, *IPD* is higher in the second step than the third step ($k_{int1} > k_{int2}$). This result indicates that diffusion resistance increased when NS diffused in the micropore of the particle due to fewer accessible sites during the third step. In turn, this explains the low

Table 5
Parameters of Sorption/Desorption of Nicosulfuron (NS) on Volcanic Ash-Derived Soils (VADS).

Parameters	COLL	MET	FRE	STB	OSN	DIG	TCO	RAL	NBR	FRU
%ads	53.47	56.42	52.05	54.12	53.61	55.56	69.94	59.39	68.83	71.41
% fast ads	92.62	90.55	95.51	93.06	92.95	90.90	76.70	87.96	79.15	77.05
% slow ads	7.38	9.45	4.49	6.94	7.05	9.10	23.30	12.04	20.8	22.95
pH_{NS}	4.76±0.01*	4.86±0.02	4.99±0.03	5.30±0.06	4.60±0.02	5.46±0.02	5.22±0.01	4.50±0.04	4.34±0.01	4.86±0.03
Linear										
K_d (mL g^{-1})	9.9±0.2	8.9±0.1	7.3±0.0	8.2±0.0	8.0±0.1	8.1±0.1	7.3±0.1	14.5±0.2	17.3±0.3	10.9±0.1
R^2	0.9961	0.9985	0.9998	0.9998	0.9988	0.9985	0.9987	0.9987	0.9972	0.9987
K_{oc}	662	386	161	161	157	140	115	210	182	99
Freundlich										
K_{fads} ($\mu g^{1-1/n}$ $mL^{1/n}$ g^{-1})	7.4±0.3	9.6±0.4	6.9±0.1	7.6±0.1	7.9±0.3	7.6±0.3	7.0±0.2	16.1±0.6	15.8±0.7	10.4±0.4
$1/n_{fads}$	1.12	0.97	1.02	1.03	1.01	1.03	1.02	0.96	1.04	1.02
R^2	0.9983	0.9988	0.9999	0.9997	0.9988	0.9988	0.9989	0.9984	0.9979	0.9989
K_{foc}	490	416	152	149	155	131	109	233	166	95
Desorption										
K_{fdes} ($\mu g^{1-1/n}$ $mL^{1/n}$ g^{-1})	78.0±0.4	76.1±0.4	72.3±0.2	74.3±0.3	70.2±0.4	83.5±0.1	70.9±0.1	125.4±0.4	134±1	107.4±0.3
$1/n_{fdes}$	0.05	0.04	0.02	0.04	0.05	0.01	0.03	0.04	0.04	0.02
R^2	0.9494	0.9426	0.9173	0.9510	0.9649	0.9654	0.9823	0.9723	0.8618	0.9520
%des	0.41	0.10	0.00	0.00	0.00	0.00	0.00	0.00	0.08	0.00
Hysteresis										
H	0.05	0.05	0.02	0.04	0.05	0.01	0.03	0.05	0.04	0.02

* Standard error.

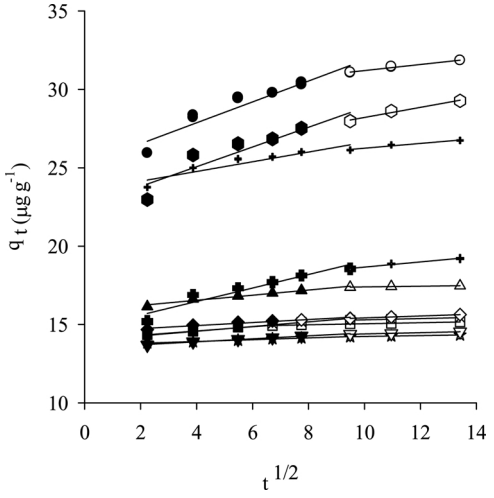

Fig. 3. Sorption kinetic of NS on VADS: COLL (□), MET (×), FRE (⋆), STB (◇), OSN (▽), DIG (△), TCO (✚), RAL (+), NBR (○) and FRU (+). Symbols represent the experimental data while lines represent the theoretical curves described by the *Intraparticle diffusion*.

diffusion rate on COLL, FRE and DIG prior to the equilibrium plateau. In contrast, TCO, RAL, NBR and FRU soils presented higher k_{int1} and k_{int2} values likely due to their mesoporous materials, which facilitated NS access to the transport pores. This result agrees with previous work associating sorption rate on porous materials and sorbent porosity (Cáceres-Jensen et al., 2013). As anticipated, only these four soils belonged to the third zone (strong initial sorption, $0.5 > R_i > 0.1$; Table 4). After initial NS sorption reached > 77 % in these soils, sorption proceeded by the *IPD* mechanism (second step (k_{int1})) (Fig. SI 6). Accordingly, TCO, NBR and FRU soils exhibited the lowest $\%fast_{ads}$ (Eq. 11, Table 3) and highest $\%slow_{ads}$ (Eq. 12, Table 3) of NS (Table 5). For all Andisols except TCO, a negative correlation was observed between *OC* and $\%fast_{ads}$, $\%fast_{ads}$ and $kint_1$ (Table SI 2) suggesting that higher *OC* decreased the fast sorption processes. In this regard, Andisols exhibited a clear trend of decreasing $\%fast_{ads}$ with increasing k_{int1}.

Additionally, A positive correlation was noted between *Silt*/*OC* and $\%fast_{ads}$, *Clay*/*OC* and $\%fast_{ads}$, $\%fast_{ads}$ and k_2, $\%fast_{ads}$ and h (Table SI 2) indicating that higher silt and clay contents increased the fast sorption processes on Ultisols and TCO. Additionally, a positive correlation was found between *OC* and $kint_1$ (Table SI 2) due to the slow diffusion of NS into the sorbent (Site, 2001), signaling a greater contribution by *IPD* on Andisols during the global sorption process. Finally, a negative correlation was exhibited between h and $kint_1$ (Table SI 2).

Both EMT and *IPD* were important mechanisms for NS sorption processes on TCO, RAL, NBR and FRU soils. For the remaining soils, results can be explained by rapid movement of NS from the exterior surface to interior surface. At that point, intramineral diffusion may occur as diffusion of NS into interlamellar regions of clay minerals on Ultisols (Brusseau and Rao, 1989). Furthermore, NS could be strongly retained on clay minerals, given the chemical characteristics of these surfaces. During the initial period (45 min), both IPD and EMT were rate-controlling steps in the retention of NS on all VADS studied. In later stages, NS sorption proceeded via a more complex mechanism consisting of both surface sorption and *IPD* within the pores.

3.3.3. Boyd equation

The calculated *Bt* values (Eq. 8, Table 3) were plotted against *t* (Fig. 4), yielding linear plots with non-zero intercepts in all cases (Table 4). *IPD* controlled the overall rate of NS on DIG, TCO, RAL NBR and FRU, as indicated by C values close to 0 and high $\%\ slow_{ads}$ (Table 4) (Boyd et al., 1947). These results are consistent with the *IPD* model (highest k_{int1} and k_{int2}). In contrast, Caceres-Jensen et. al. (Caceres-Jensen et al., 2013) observed intercept values close to zero for DI on the same VADS, signaling that pore diffusion controls the rate of MT and limits the sorption rate of DI. This distinction from NS can be explained in part by the nonionic chemical structure of DI.

A positive correlation was found between *C* and k_2 as well as *C* and h (Table SI 2) indicating that the $\%fast_{ads}$ increased with the distance of the intercept from zero. In contrast, a negative correlation was exhibited between *C* and $kint_1$ (Table SI 2). The highest intercepts (C values between 2.1 and 2.7 and slowest $\%\ slow_{ads}$; Table 4) were documented on the soils with lowest *OC* content (COLL, MET, FRE, STB and OSN). In this sense, the step controlling the overall rate of MT on these soils is Film Diffusion or chemisorption in the beginning of the sorption process (Caceres-Jensen et al., 2013). This finding suggests that in VADS with low OC content, kinetics were governed principally by Liquid Film Diffusion or chemisorption complementarily with EMT of NS from the bulk solution to the surface soil paired with *IPD* into macro and micropores. Conditions that foster Liquid Film Diffusion

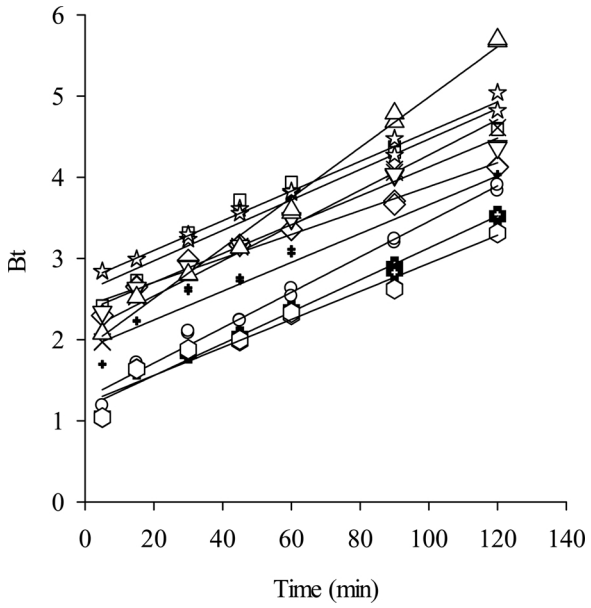

Fig. 4. Sorption kinetic of NS on VADS: COLL (□), MET (×), FRE (⋆), STB (◇), OSN (▽), DIG (△), TCO (✚), RAL (+), NBR (○) and FRU (+). Symbols represent the experimental data while lines represent the theoretical curves described by the Boyd Model.

control of the overall sorption rate include low degree of agitation, low solution concentration and small solute size (Valderrama et al., 2008).

3.3.4. Two-site nonequilibrium (TSNE) model

This model (Eq. 9, Table 3) described all sorption kinetics data and experimental K_d values ($R^2 > 0.9509$, Table 4). Fig. 5 shows nonlinear plots of C/C_i versus t (h). Concentration decay curves illustrate an initial step of rapid NS uptake on TCO, NBR and FRU as indicated by the high k_s values (Table 4). During the second step, uptake steadily increased until equilibrium conditions. The F fraction was highest on COLL, MET, FRE, STB, OSN and DIG soils (Table 4), where > 83 % of sites corresponded to the initial phase in which equilibrium was quickly achieved. In contrast, this fraction was more time-dependent on TCO, RAL, NBR and FRU (F values between 53 and 76 %). A positive correlation was found between %Type 1 sites and k_2 as well as %Type 1 sites and h (Table SI 2). On the other hand, a negative correlation was exhibited between h, $\%fast_{ads}$ and C with respect to k_s (Table SI 2). A positive correlation was found between k_{int1} and K with respect to k_s and between % Type 1 sites and C with respect to k_{des} (Table SI 2). As such, the high OC content in TCO, NBR and FRU (Table 1) allowed an increase of IPD path length (highest $\%\ \text{slow}_{\text{ads}}$ and k_{int1} ; Table 4 and 5) where a lower value of k_2 could be expected for NS sorption (Table 4). The reason for this behavior may be slower sorption by means of slow diffusion transfer of the sorbate within the organic matrix or on sorption sites inaccessible to water, which is a function of the square root of time (Site, 2001). Specifically, the OM and Al/Fe oxides in VADS promote aggregate formation, impacting soil porosity. In turn, this characteristic impacts the chemical associations and physical properties (Ruiz et al., 2010). In this sense, NBR presented the most suitable conditions for NS sorption because of its positive surface charge interacting with the anionic species at the pH of the bulk solution (Table 1). For hydrophobic or low polarity organic compounds, intra-OM diffusion is the most probable intra-sorbent diffusion-related mechanism (Brusseau and Rao, 1989), which can occur during the transport of pesticides in soils (Brusseau and Rao, 1989). In general, NS sorption on VADS occurred mainly on highly accessible sites (F > 53 %) (Table 4) increasing the h values of NS on VADS ($C_1 \approx q_{max}$; Ri < 0.04 and RE < 0.055) (Tables 4 and SI3). The best kinetic model of NS in VADS as well their transport mechanisms are schematically represented in Fig. 6. The potential for groundwater contamination would be lowest in VADS with low F values.

3.4. Sorption models

Data for sorption of NS on all soils were well described by the *Freundlich* model (Eq. 14, Table 3) with $R^2 \geq 0.9986$ (K_{fads} values between 6.9 and 16.1 $\mu g^{1-1/n}\, mL^{1/n}\, g^{-1}$, Table 5). The $1/n_{fads}$ values were lower than 1 on MET (dominant mineral: halloysite; Table 1) and RAL (trace fraction mineral: montmorillonite; Table 1) indicating that NS sorption proceeded on highly energetic heterogeneous sorption sites (Gonzalez and Ukrainczyk, 1996), followed by the low energy sites with increased surface concentration (Site, 2001; Okada et al., 2016), for which k_{des} values were the slowest (Table 4). All Andisols except RAL showed $1/n_{fads}$ values greater than 1, showing a strong intermolecular attraction of NS within of minerals layers (Site, 2001).

The RAL and NBR soils showed the highest K_f values for NS due to their high OC content and acidic pH (Fuentes et al., 2014). The pH of Andisols would be the sole favorable situation for hydrophobic interactions of NS- OM because of the fraction of neutral acid species present (Tables 1 and 5). The quantity and quality of OM and minerals has been shown to influence the sorption of pesticides including SUs on permanent charge soils and variable-charge soils (Caceres-Jensen et al., 2018, 2019; Azcarate et al., 2015; Hyun and Lee, 2004, 2005) (Table SI 1). In contrast, NS was almost completely in the anionic form in the equilibrium solutions of COLL, FRE, TCO, and STB soils (Table 5). Accordingly, little to no sorption would be expected according to the IEP of VADS (lower value than the corresponding pH_{H_2O}, Table 1). In this sense, the anionic herbicide was adsorbed principally on VADS that present negative net charge according to the pK_a value of NS (Table 2), the pH of the soil, and the IEP (Table 1).

In our study, a wide range of K_{foc} (94–490) values was observed, indicating that NS was not exclusively adsorbed on OM (Table 5). In this regards, ionic interactions contributed in some degree to anionic herbicide sorption on VADS (Caceres-Jensen et al., 2018). These finding broadly supports previous studies in this area linking CEC, Surface area, OC, silt and clay content with sorption process on soils containing predominantly 2:1 clay minerals (Table SI 1) (Fernández-Bayo et al., 2008; Oliveira et al., 2001). Taken together, these observations confirm that these are important factors influencing the initial sorption on external sites (positive correlation between C_1 and K_f; Tables SI 1 and SI 2). If the ratio of mineral to OC fraction is > 30, ionic interactions are maximized (Spadotto and Hornsby, 2003; Villaverde et al., 2008). The

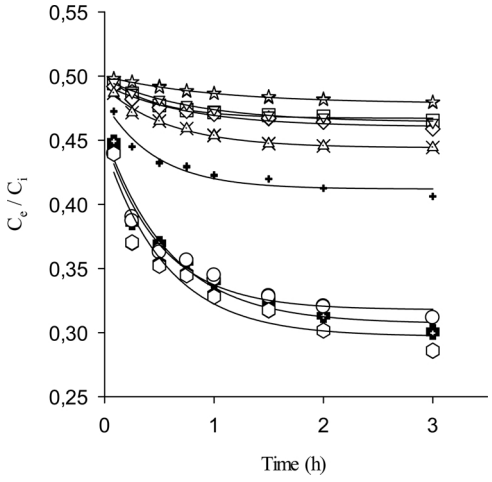

Fig. 5. Sorption kinetic of NS on VADS: COLL (□), MET (×), FRE (⋆), STB (◇), OSN (▽), DIG (△), TCO (✚), RAL (+), NBR (○) and FRU (+). Symbols represent the experimental data while lines represent the theoretical curves described by the *Two-site non-equilibrium model* (*TSNE*).

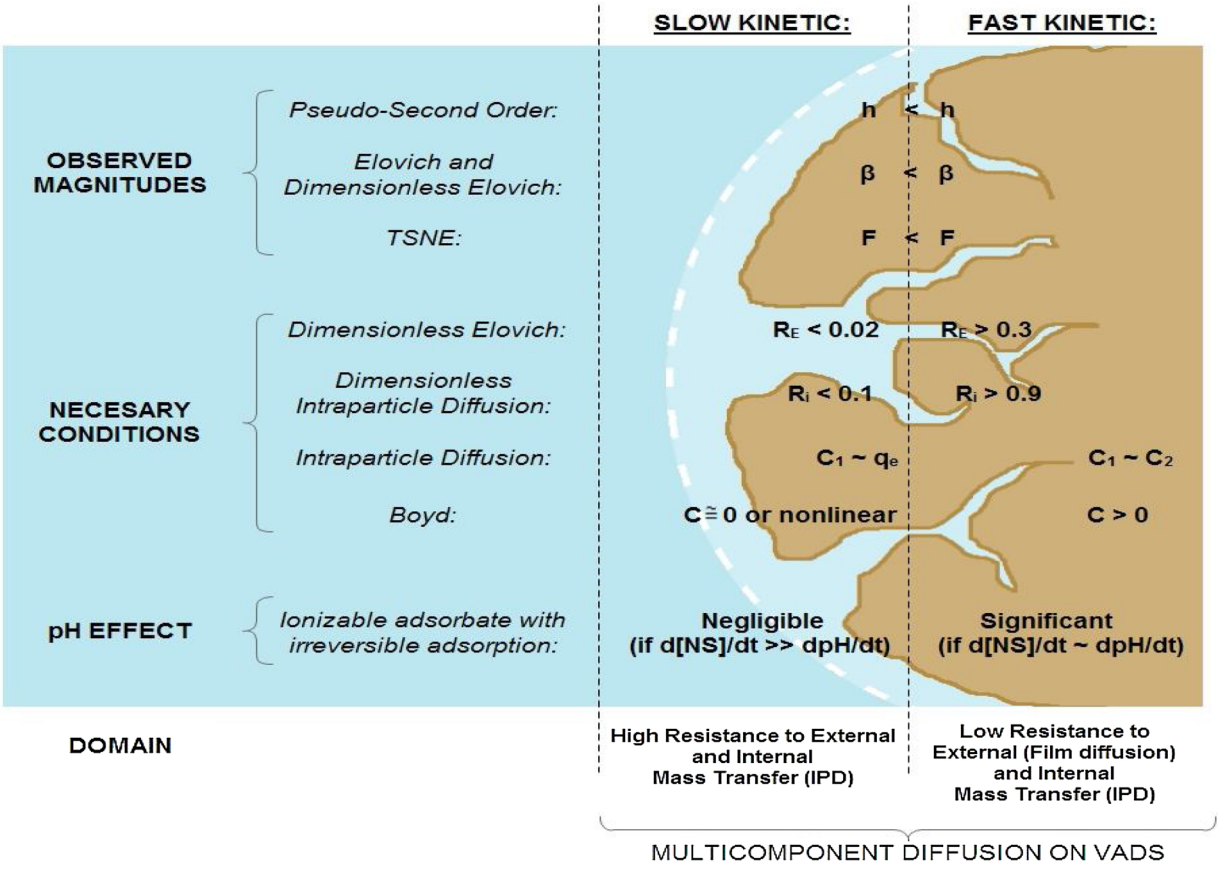

Fig. 6. General scheme for kinetic sorption of NS on VADS.

Ultisols studied herein present similar properties than tropical soils (mineral composition based on goethite, gibbsite, hematite and 1:1 clays such as kaolinite, with low *OM* content and low *pH*) (Table SI 1). Our Ultisols studied herein present a higher mineral contribution (ratio between 15.3 and 30.5, Table 1), a significant contribution of clay minerals on NS sorption might be expected, particularly on soils with low *OC* content and high clay content (Ukrainczyk and Rashid, 1995). The dominant crystalline mineral present on COLL is kaolinite (Table 1). Crystalline minerals such as halloysite and kaolinite are non-expandable 1:1 clay minerals and present a low *CEC* (Joussein et al., 2005). Since the *IEP* for kaolinite is between 3 and 4, the net charge would be negative at the pH of COLL, discouraging electrostatic interactions with NS and consequently NS sorption. Thus, kaolinite and the low *OC* content of COLL contributed to the low sorption of NS and increased mobility of NS in Ultisols. (Ukrainczyk and Rashid, 1995) studied the sorption-desorption of NS on calcium montmorillonite, calcium hectorite, silica, and ferrihydrite (Ukrainczyk and Rashid, 1995). The sorption isotherms on all sorbents had a linear behavior, demonstrating strong sorption only on the layer silicate mineral compared to less sorption on oxides. These researchers suggested attributed the strong sorption to the zwitterion form of NS present in solution, which features a protonated nitrogen. Another less likely explanation is rapid hydrolysis catalyzed by the surface acidity of clay minerals. This would result in strong sorption on clays of the resulting basic product. One of the NS hydrolysis products, 2-amino-4,6-bis(dimethoxy)-pyrimidine, is similar to aniline, which is strongly adsorbed on silicate layers. The NS sorption was low on silica and buserite (layered manganese oxide) despite having large surface area and high CEC.

The *Freundlich* model fit experimental data well ($R^2 \geq 0.9986$, Table 5), with the *H* coefficient close to zero for all VADS. This effect was more pronounced in FRE, DIG, TCO and FRU soils. These results suggest that NS reincorporation to the soil solution during desorption must be negligible. Slow rates of NS desorption paired with pore structure heterogeneity potentiated a marked irreversible NS sorption on FRE (lowest k_{des} and *H* values; Tables 4 and 5) due to the entrapment of adsorbed NS on microporous mineral surfaces or on *OM* within FRE soil aggregates (Caceres-Jensen et al., 2009). This hysteresis phenomenon can be explained by stronger interactions through metal binding compared to weaker hydrophobic and electrostatic interactions, and was corroborated with negligible *%des* (Table 5). A different behavior was observed on COLL (lowest *OC* content; Table 1) which exhibited the highest k_{des} and *H* values, translating to less favorable conditions for NS sorption. Abdullah et al. (2001) obtained a high MSM desorption on agricultural soils with low *OM*, indicating the potential for MMS leaching through the soil profile contaminating groundwater (Abdullah et al., 2001).

The *IPD* model for pesticides in these VADS predicts that sorption equilibrium will be attained later in the soil with stronger sorption capacity. Similarly, a strongly adsorbed pesticide will take longer to achieve sorption equilibrium than one that is weakly adsorbed (Villaverde et al., 2009). For Andisols, NS will take longer to achieve sorption equilibrium on TCO, NBR and FRU soils (lowest *H*, *F* and *h* values, and highest $t_{1/2}$ values; Tables 4 and 5). However, NS will present the lowest bioavailability in the soil solutions of RAL, (highest k_f, *F* and *h* values; lowest $t_{1/2}$; and low *H* value; Tables 4 and 5), which exhibited low biocidal action due to low absorption by the plant. On the other hand, FRE soil will present the highest bioavailability in the solution, favoring both biotic and abiotic dissipation (lowest K_f; highest *F* and *h* values; Tables 4 and 5).

PCA and cluster analysis of soil characteristics (*OC* (%), *CEC*, Sand/ *OC*, Silt/ *OC*, Clay/ *OC*, *IEP* and pH_{NS}, Tables 1 and 5) grouped VADS into three clusters: 1) Ultisols characterized by textures with high values of Sand/ *OC*, Silt/ *OC* and Clay/ *OC* and sorption localized to the positive region of PC1 (Fig. 1a–b); 2) Andisols with high *CEC* values

and low acidity fell positively on PC2 in a similar extent. These VADS have moderate values for Sand/ *OC*, Silt/ *OC* and Clay/ *OC* and *OC* and display moderate sorption capacities by soils constituents different from *OC* ; and 3) Andisols with high and medium influence of *OC* on their sorption capacities localized to the negative and close to zero regions of PC1. Fig. 1b illustrates that the *CEC* and pH_{NS} vectors (PC2) are orthogonal to the ratio of *mineral*/*OC* and *OC* vectors (PC1) indicating that these PC2 variables are uncorrelated with NS sorption by soils constituents different from *OC*. This type of NS sorption is highly correlated with VADS texture. The fact that Ultisols presented higher K_{fOC} values was supported by presence of inorganic soil constituents. Fig. 1c displays score plots of PC1 and PC3 of the PCA, where COLL, MET, TCO and FRU are grouped and show similar PC3 eigenvalues. This result reveals that TCO and FRU (to a lesser extent) have compensatory properties (ie. IEP, pH_{NS}, CEC, silt and clay contents; Fig. 1d).

Finally, the values of Silt%, OC, pH_{NS} and CEC isolines were established with the interpolated values obtained for each VADS station (Figs. 7 and SI 7). The Fig. 7 shows the spatial distribution of K_f values of NS on VADS, which increase with latitude. NBR and RAL, located in the southern zone, exhibit the maximum K_f values. Higher OC content (Table 1) could enhance NS sorption on Andisols. In general, plotting K_f values across space yielded three zones: 1) the sector between DIG and STB stations ($K_f < 7.9$); 2) the sector between COLL and FRE stations ($7.9 \leq K_f \leq 9.9$); and 3) the sector between NBR and RAL stations ($K_f \geq 10$). As a whole, the spatial model reveals an association between K_f and OC -interpolated values of DEM in relation to latitude.

4. Conclusions

In this work, the *PSO* model generally fit the experimental kinetics data well, confirming chemisorption of NS onto VADS particles. The k_2 and h values illustrated the different behavior of NS on VADS. The *IPD* model indicated differences in the extent of sorption for VADS with % *OC* slower than 5.8, where film diffusion and EMT across the boundary layer are the processes controlling NS sorption during the fast phase. The characteristic curves obtained through the *IPD* model classified NS-

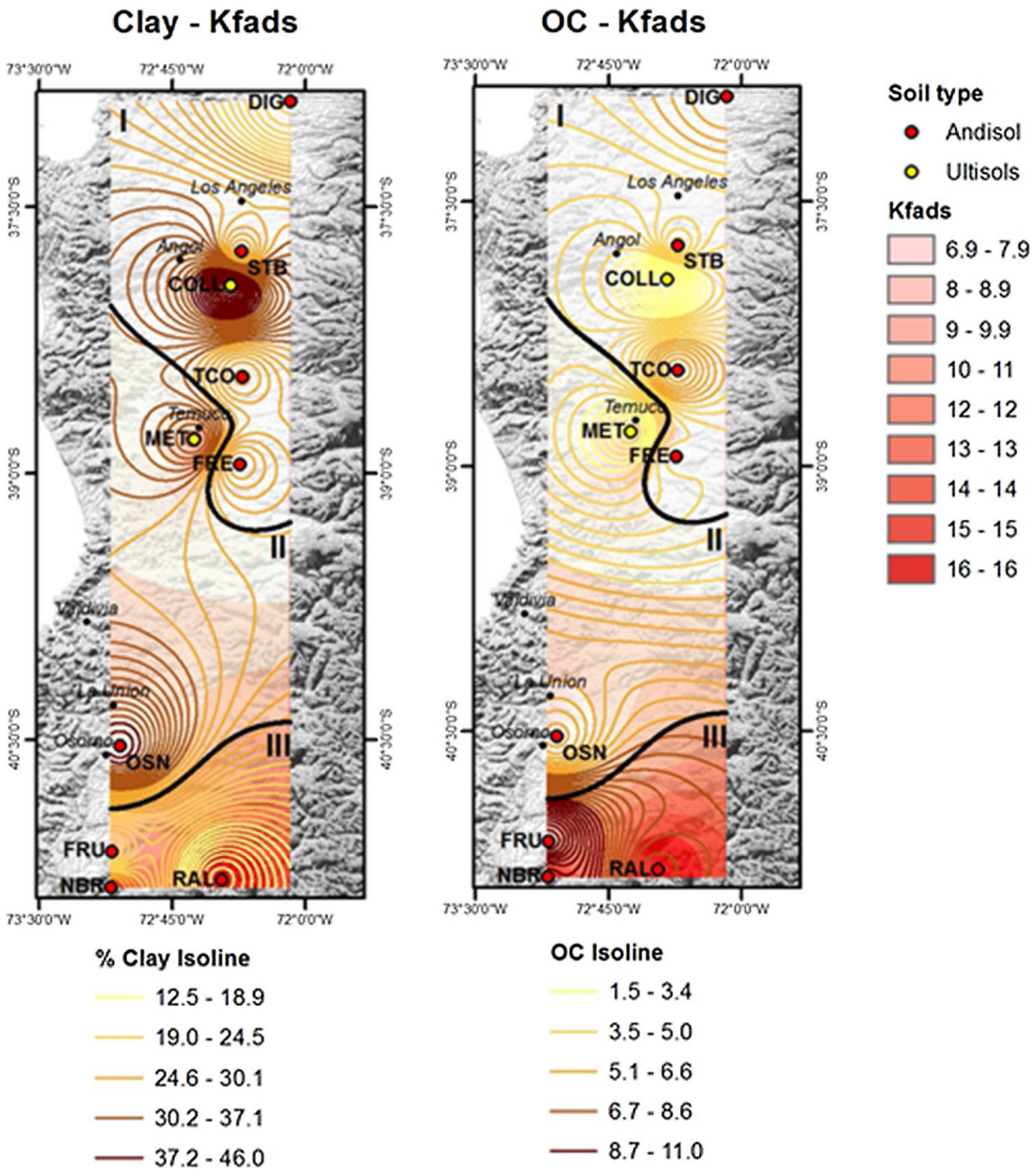

Fig. 7. Spatial distribution of K_f values of NS on VADS.

soil systems within the zone of rapidly rising initial sorption and strongly initial sorption, respectively. The *Boyd* model indicated that NS sorption in VADS with low *OC* content was related to film diffusion or chemisorption. In total, however, the *TSNE* model proved to be the best solute sorption mechanism model for VADS, including an initial phase where > 53 % of sites accounted for instantaneous sorption and rapid equilibrium achievement.

The equilibrium data fitted by the *Freundlich* model confirmed the heterogeneity of VADS and signaled a strong intermolecular attraction of NS within the minerals. The higher content of *OC* and allophane are the factors governing *IPD* in Andisols. The presence of kaolinite, halloysite, montmorillonite and Al/Fe oxides in Ultisols were significant in NS sorption during the initial phase by film diffusion and ETM mechanism. In light of the slow sorption rate exhibited by NS on VADS with low *F* values and located in regions with high rainfall intensity, the relevant mechanism and the low sorption capacity must be considered to assess the leaching behavior of NS. As a whole, the present work adds to our still limited understanding of the chemisorption of herbicides in VADS. Further research should focus on the environmental fate of SUs in Ultisols using both transport and QSAR models to predict sorption on VADS and related environmental consequences.

Declaration of Competing Interest

The authors declare that they have no known competing financial interests or personal relationships that could have appeared to influence the work reported in this paper.

The authors declare the following financial interests/personal relationships which may be considered as potential competing interests.

Acknowledgements

This study was supported through 06-2019-APIX (DIUMCE project, Chile), FONDECYT-11110421 (CONICYT, Chile) and FONDECYT-11100308 (CONICYT, Chile), FCHA/DOCTORADO NACIONAL/2017-21170499 (CONICYT, Chile), Basal Funding for Scientific and Technological Centers of Excellence, FB0807 (CEDENNA). We thank Alyssa Grube for assistance in language support.

Appendix A. Supplementary data

Supplementary material related to this article can be found, in the online version, at doi:https://doi.org/10.1016/j.jhazmat.2019.121576.

References

Abdullah, R., Saraswathy, S., Norhayati, M.T., 2001. Adsorption-desorption behaviour of metsulfuron methyl in selected Malaysian agricultural soils. Fresenius Enviromental Bulletin 10, 94–97.
Allison, L.E., 1965. Organic carbon. In: Black, C.A., Evans, D.D., White, J.L., Ensminger, L.E., Clark, F.E. (Eds.), Methods of Soil Analysis, Part 2. Agronomy Series. ASA, Madison, WI, pp. 1367–1396.
Appel, J., 1973. Freundlich's adsorption isotherm. Surf. Sci. 39, 237–244.
Ayranci, E., Hoda, N., 2005. Adsorption kinetics and isotherms of pesticides onto activated carbon-cloth. Chemosphere 60, 1600–1607.
Azcarate, M.P., Montoya, J.C., Koskinen, W.C., 2015. Sorption, desorption and leaching potential of sulfonylurea herbicides in Argentinean soils. J. Environ. Sci. Health B 50, 229–237.
Azizian, S., 2004. Kinetic models of sorption: a theoretical analysis. J. Colloid Interface Sci. 276, 47–52.
Blake, G.R., 1965. Particle density. In: Black, C.A. (Ed.), Methods of Soil Analysis. Part 1. Physical and Mineralogical Properties, Including Statistics of Measurement and Sampling. American Society of Agronomy, Soil Science Society of America, Madison, WI, pp. 371–373.
Boyd, G.E., Adamson, A.W., Myers, L.S., 1947. The exchange adsorption of ions from aqueous solutions by organic zeolites. Ii. Kinetics1. J. Am. Chem. Soc. 69, 2836–2848.
Brown, H.M., 1990. Mode of action, crop selectivity, and soil relations of the sulfonylurea herbicides. Pest Manag. Sci. 29, 263–281.
Brusseau, M.L., Rao, P.S.C., 1989. The influence of sorbate-organic matter interactions on sorption nonequilibrium. Chemosphere 18, 1691–1706.
Caceres, L., Fuentes, R., Escudey, M., Fuentes, E., Baez, M., 2010. Metsulfuron-methyl sorption/desorption behavior on volcanic ash-derived soils. Effect of phosphate and ph. J. Agric. Food Chem. 58, 6864–6869.
Cáceres-Jensen, L., 2010. Modelación de la dinámica de glifosato y metil-metsulfurón en suelos derivados de cenizas volcánicas, in: Facultad de Química y Biología. Universidad de Santiago de Chile. Doctor en Química, Santiago.
Caceres-Jensen, L., Gan, J., Báez, M., Fuentes, R., Escudey, M., 2009. Adsorption of glyphosate on variable-charge, volcanic ash-derived soils. J. Environ. Qual. 38, 1449–1457.
Cáceres-Jensen, L., Escudey, M., Fuentes, E., Báez, M.E., 2010. Modeling the sorption kinetic of metsulfuron-methyl on andisols and ultisols volcanic ash-derived soils: kinetics parameters and solute transport mechanisms. J. Hazard. Mater. 179, 795–803.
Caceres-Jensen, L., Rodriguez-Becerra, J., Parra-Rivero, J., Escudey, M., Barrientos, L., Castro-Castillo, V., 2013. Sorption kinetics of diuron on volcanic ash derived soils. J. Hazard. Mater. 261, 602–613.
Caceres-Jensen, L., Rodriguez-Becerra, J., Escudey, M., 2018. Impact of physical/chemical properties of volcanic ash-derived soils on mechanisms involved during sorption of ionisable and non-ionisable herbicides. In: Edebali, D.S. (Ed.), Advanced Sorption Process Applications. Intech, London, pp. 95–149.
Caceres-Jensen, L., Neira-Albornoz, A., Escudey, M., 2019a. Herbicides mechanisms involved in the sorption kinetic of ionisable and non ionisable herbicides: impact of physical/chemical properties of soils and experimental conditions. In: Rahman, R.O.A. (Ed.), Kinetic Modeling for Environmental Systems. IntechOpen, London.
Caceres-Jensen, L., 2019b. Electrochemical method to study the environmental behavior of Glyphosate on volcanic soils: Proposal of adsorption-desorption and transport mechanisms. J. Hazard. Mater. 379, 120746.
Denton, O.A., Aduramigba-Modupe, V.O., Ojo, A.O., Adeoyolanu, O.D., Are, K.S., Adelana, A.O., Oyedele, A.O., Adetayo, A.O., Oke, A.O., 2017. Assessment of spatial variability and mapping of soil properties for sustainable agricultural production using geographic information system techniques (gis). Cogent Food Agric. 3, 1279366.
Escudey, M., Galindo, G., Forster, J.E., Briceño, M., Diaz, P., Chang, A., 2001. Chemical forms of phosphorus of volcanic ash-derived soils in chile. Commun. Soil Sci. Plant Anal. 32, 601–616.
Fernández-Bayo, J.D., Nogales, R., Romero, E., 2008. Evaluation of the sorption process for imidacloprid and diuron in eight agricultural soils from southern europe using various kinetic models. J. Agric. Food Chem. 56, 5266–5272.
Fuentes, R., Henríquez, J., Pinochet, D., Clunes, J., 2014. Variación de la biodisponibilidad de los herbicidas metsulfuron - metil y triasulfuron bajo distintas condiciones de encalado en dos suelos volcánicos del sur de chile. Agro Sur 42, 10.
Gonzalez, J.M., Ukrainczyk, L., 1996. Adsorption and desorption of nicosulfuron in soils. J. Environ. Qual. 25, 1186–1192.
Hameed, B.H., El-Khaiary, M.I., 2008. Equilibrium, kinetics and mechanism of malachite green adsorption on activated carbon prepared from bamboo by k2co3 activation and subsequent gasification with co2. J. Hazard. Mater. 157, 344–351.
Ho, Y.-S., 2006. Review of second-order models for adsorption systems. J. Hazard. Mater. 136, 681–689.
Huentemilla, M.C., 2015. Predicción de transporte de nicosulfurón en suelos derivados de ceniza volcánica utilizando stanmod y hidrus-1d"., Profesor de Química y Estadística.
Hyun, S., Lee, L.S., 2004. Factors controlling sorption of prosulfuron by variable-charge soils and model sorbents. J. Environ. Qual. 33, 1354–1361.
Hyun, S., Lee, L.S., 2005. Quantifying the contribution of different sorption mechanisms for 2,4-dichlorophenoxyacetic acid sorption by several variable-charge soils. Environ. Sci. Technol. 39, 2522–2528.
Inoue, M.H., Oliveira, R.S., Regitano, J.B., Tormena, C.A., Constantin, J., Tornisielo, V.L., 2004. Sorption kinetics of atrazine and diuron in soils from southern brazil. J. Environ. Sci. Health B 39, 589–601.
Ioannou, Z., Simitzis, J., 2009. Adsorption kinetics of phenol and 3-nitrophenol from aqueous solutions on conventional and novel carbons. J. Hazard. Mater. 171, 954–964.
Joussein, E., Petit, S., Churchman, J., Theng, B., Righi, D., Delvaux, B., 2005. Halloysite Clay Minerals - a Review.
Kah, M., Brown, C.D., 2006. Adsorption of ionisable pesticides in soils. Reviews of Environmental Contamination and Toxicology, vol 188. Springer, New York, pp. 149–217.
Köhne, J.M., Köhne, S., Simunek, J., 2009. A review of model applications for structured soils: B) pesticide transport. J. Contam. Hydrol. 104, 36–60.
Kumar, K.V., Ramamurthi, V., Sivanesan, S., 2005. Modeling the mechanism involved during the sorption of methylene blue onto fly ash. J. Colloid Interface Sci. 284, 14–21.
Maqueda, C., Undabeytia, T., Villaverde, J., Morillo, E., 2017. Behaviour of glyphosate in a reservoir and the surrounding agricultural soils. Sci. Total Environ. 593, 787–795.
Nkedi-Kizza, P., Shinde, D., Savabi, M.R., Ouyang, Y., Nieves, L., 2006. Sorption kinetics and equilibria of organic pesticides in carbonatic soils from south florida. J. Environ. Qual. 35, 268–276.
Okada, E., Costa, J.L., Bedmar, F., 2016. Adsorption and mobility of glyphosate in different soils under no-till and conventional tillage. Geoderma 263, 78–85.
Oliveira, R.S., Koskinen, W.C., Ferreira, F.A., 2001. Sorption and leaching potential of herbicides on Brazilian soils. Weed Res. 41, 97–110.
Önal, Y., 2006. Kinetics of adsorption of dyes from aqueous solution using activated carbon prepared from waste apricot. J. Hazard. Mater. 137, 1719–1728.
Pizarro, C., Escudey, M., Fabris, J., 2003. Influence of organic matter on the iron oxide mineralogy of volcanic soils. Hyperfine Interact. 148–149, 53–59.
Pojananukij, N., Wantala, K., Neramittagapong, S., Lin, C., Tanangteerpong, D., Neramittagapong, A., 2017. Improvement of as(iii) removal with diatomite overlay

nanoscale zero-valent iron (nzvi-d): adsorption isotherm and adsorption kinetic studies. Water Sci. Technol. Water Supply 17, 212–220.
Riahi, K., Chaabane, S., Thayer, B.B., 2017. A kinetic modeling study of phosphate adsorption onto phoenix dactylifera l. Date palm fibers in batch mode. J. Saudi Chem. Soc. 21, S143–S152.
Rivera, A., Bown, F., Carrión, D., Zenteno, P., 2012. Glacier responses to recent volcanic activity in southern chile. Environ. Res. Lett. 7, 014036.
Robinson, T.P., Metternicht, G., 2006. Testing the performance of spatial interpolation techniques for mapping soil properties. Comput. Electron. Agric. 50, 97–108.
Rudzinski, W., Panczyk, T., 2000. Kinetics of isothermal adsorption on energetically heterogeneous solid surfaces: a new theoretical description based on the statistical rate theory of interfacial transport. J. Phys. Chem. B 104, 9149–9162.
Ruiz, B., Cabrita, I., Mestre, A.S., Parra, J.B., Pires, J., Carvalho, A.P., Ania, C.O., 2010. Surface heterogeneity effects of activated carbons on the kinetics of paracetamol removal from aqueous solution. Appl. Surf. Sci. 256, 5171–5175.
Sabadie, J., 2002. Nicosulfuron: Alcoholysis, chemical hydrolysis, and degradation on various minerals. J. Agric. Food Chem. 50, 526–531.
Shinohara, H., Witter, J.B., 2005. Volcanic gases emitted during mild strombolian activity of villarrica volcano, chile. Geophys. Res. Lett. 32, 1–5.
Shoji, S., Takahashi, T., 2002. Environmental and agricultural significance of volcanic ash soils. Glob. Environ. Res.-Eng. Ed.edition 6, 113–135.
Site, A.D., 2001. Factors affecting sorption of organic compounds in natural sorbent/water systems and sorption coefficients for selected pollutants. A review. J. Phys. Chem. Ref. Data 30, 187–439.
Spadotto, C.A., Hornsby, A.G., 2003. Soil sorption of acidic pesticides: modeling ph effects. J. Environ. Qual. 32, 949–956.
Sparks, D.L., 2003. 5 - Sorption Phenomena on Soils, in: Environmental Soil Chemistry, Second edition. Academic Press, Burlington, pp. 133–186.
Stern, C.R., 2004. Active andean volcanism: its geologic and tectonic setting. Rev. Geol. Chile 31, 161–206.
Takahashi, T., Shoji, S., 2002. Distribution and classification of volcanic ash soils. Glob. Environ. Res.-Eng. Ed. 6, 83–98.
Tan, K.L., Hameed, B.H., 2017. Insight into the adsorption kinetics models for the removal of contaminants from aqueous solutions. J. Taiwan Inst. Chem. Eng. 74, 25–48.
Tournebize, J., Passeport, E., Chaumont, C., Fesneau, C., Guenne, A., Vincent, B., 2013. Pesticide de-contamination of surface waters as a wetland ecosystem service in agricultural landscapes. Ecol. Eng. 56, 51–59.
Ukrainczyk, L., Rashid, N., 1995. Irreversible sorption of nicosulfuron on clay-minerals. J. Agric. Food Chem. 43, 855–857.
Valderrama, C., Gamisans, X., de las Heras, X., Farrán, A., Cortina, J.L., 2008. Sorption kinetics of polycyclic aromatic hydrocarbons removal using granular activated carbon: intraparticle diffusion coefficients. J. Hazard. Mater. 157, 386–396.
Valenzuela Riquelme, C., Cáceres-Jensen, L., Rodríguez Becerra, J., 2010. Antecedentes relevantes en la generación de un modelo qsar para la predicción de pesticidas en suelos volcánicos, Facultad de Ciencias Básicas. Universidad Metropolitana de Ciencias de la Educación. Licenciatura en Educación Química y Pedagogía en Química mención Educación en Astronomía, Santiago.
Vergara, M., López-Escobar, L., Palma, J.L., Hickey-Vargas, R., Roeschmann, C., 2004. Late tertiary volcanic episodes in the area of the city of santiago de chile: new geochronological and geochemical data. J. South Am. Earth Sci. 17, 227–238.
Villaverde, J., Kah, M., Brown, C.D., 2008. Adsorption and degradation of four acidic herbicides in soils from southern Spain. Pest Manag. Sci. 64, 703–710.
Villaverde, J., van Beinum, W., Beulke, S., Brown, C.D., 2009. The kinetics of sorption by retarded diffusion into soil aggregate pores. Environ. Sci. Technol. 43, 8227–8232.
Wankasi, D., Horsfall, M., Spiff, A.I., 2006. Sorption kinetics of pb2+ and cu2+ ions from aqueous solution by nipah palm (nypa fruticans wurmb) shoot biomass. Electron. J. Biotechnol. 9, 587–592.
Wu, F.-C., Tseng, R.-L., Juang, R.-S., 2009a. Characteristics of Elovich equation used for the analysis of adsorption kinetics in dye-chitosan systems. Chem. Eng. J. (Lausanne) 150, 366–373.
Wu, F.-C., Tseng, R.-L., Juang, R.-S., 2009b. Initial behavior of intraparticle diffusion model used in the description of adsorption kinetics. Chem. Eng. J. (Lausanne) 153, 1–8.
Yu, X., Pan, L., Ying, G., Kookana, R.S., 2010. Enhanced and irreversible sorption of pesticide pyrimethanil by soil amended with biochars. J. Environ. Sci. 22, 615–620.